ELSEVIER

Journal of Nuclear Materials 317 (2003) 93–101

journal of nuclear materials

www.elsevier.com/locate/jnucmat

Swelling rate versus swelling correlation in 20% cold-worked 316 stainless steels

S. Ukai *, T. Uwaba

O-arai Engineering Center, Japan Nuclear Cycle Development Institute, 4002, Narita, O-arai, Ibaraki prefecture, 311-1393, Japan

Received 23 July 2001; accepted 15 December 2002

Abstract

A quantitative correlation of the swelling rate versus swelling is presented. Swelling data of 20% cold-worked 316 stainless steels were analyzed using the power law swelling equation. The prolonged transient region with keeping the suppressed swelling rate was clearly demonstrated for the improved 316 stainless steels like PNC316 and 316Ti. Rate theory analyses lead to the role of precipitates as point defect sinks for retardation of the void growth.

PACS: 61.80

1. Introduction

The radiation-induced void swelling is a life limiting factor for 316 austenitic stainless steel that is used as fuel cladding of fast breeder reactors as well as structure materials of light water reactors. The swelling behavior can be conveniently described as a low-swelling transient period followed by an acceleration to a region of nearly linear swelling of about 1%/dpa [1]. Once the steady state linear swelling is attained, the materials cannot be used in reactors: upper band of swelling applicable to the fuel cladding may be ranged less than 10–15%. Thus, designers require the accurate swelling trend and values during the transient region. Such behavior is shown schematically in Fig. 1. The commercial stainless steels take the prolonged transient region approaching a linear swelling rate, thus a curvature in the transient swelling region should be significantly important from the design viewpoint. This feature is characterized by the swelling rate versus swelling relation in the transient region. The information is, however, very limited [2]. In the commercial stainless steels, nucleation and growth of voids concomitantly occur in the transient region, and affect significantly the swelling behavior.

In the present study, we construct the swelling rate–swelling correlation within the transient swelling region using irradiation data acquired in Japan Nuclear Cycle Development Institute (JNC) and published in literatures. In order to clarify the deduced correlation for swelling behavior, microstructure changes affecting void growth through sink balance between dislocation, void and precipitates are interpreted in terms of rate theory analyses.

2. Power law swelling equation

P,Ti modified 316 stainless steel, which was developed by JNC to improve the swelling resistance and designated PNC316 [3], was irradiated in JOYO MK-II core and FFTF as the fuel pin claddings [4]. A nominal chemical composition of PNC316 is Fe–16Cr–14Ni–0.05C–2.5Mo–0.7Si–0.025P–0.004B–0.1Ti–0.1Nb. Solution annealing was performed at a temperature around 1080 °C, followed by 20% cold working. The dimension of the fuel pin claddings of the MONJU type is 6.5 mm in diameter and 0.47 mm in thickness. After completion

* Corresponding author. Tel.: +81-29 267 4141x5711; fax: +81-29 266 2904/267 7130.

E-mail address: uki@oec.jnc.go.jp (S. Ukai).

0022-3115/03/$ - see front matter
doi:10.1016/S0022-3115(02)01703-8

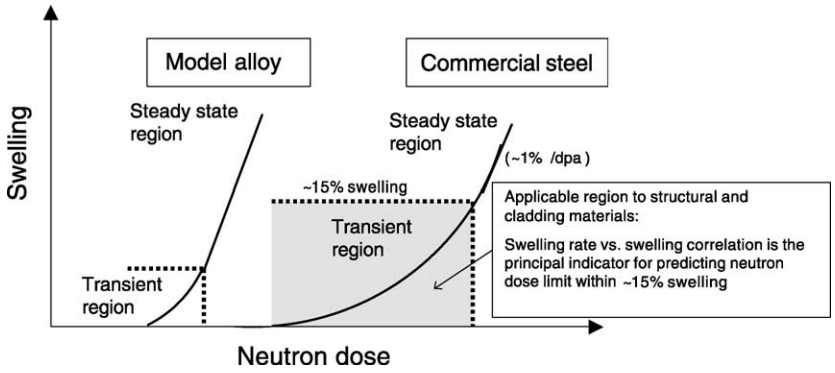

Fig. 1. Schematic view of neutron dose dependence of swelling for commercial austenitic stainless steels (AISI 316) and related ternary model alloys (Fe–Cr–Ni).

of irradiation, the fuel pins were cut into 80 mm length segments, and each segment was defueled by mechanical and chemical treatment. The density measurement was conducted for the defueled segments.

In Fig. 2(a), results of swelling measurement of PNC316 are exhibited in the linear relationship of neutron dose versus swelling in the temperature range of 465–505 °C. The swelling data lie 0.58–6.3% in the range of neutron dose of 87–107 dpa, which is recognized as being still in the swelling transient region approaching to the steady state. It is thus not easy to interpret the dose dependence of swelling with the available swelling data up to 107 dpa, and to extrapolate to the predicted swelling values at higher neutron dose of 120 dpa.

It is well known that swelling is represented by means of power law swelling equation [5],

$$\Delta V/Vo = m_1(\phi t - m_2)^n, \tag{1}$$

where $\Delta V/Vo$ is the volumetric swelling, ϕt is the neutron dose in dpa, m_1, m_2 and n are material coefficients. Taking logarithm of both side in Eq. (1), volumetric swelling versus neutron dose is expressed in linear relationship, and n value can be derived from the slope of this relation. Fig. 2(b) shows the log–log plot of the volumetric swelling versus neutron dose within the swelling transient region. In this analysis, the m_2 was selected as 83 dpa, which corresponds to the neutron dose just initiating void swelling, so as to minimize the standard deviation using a regression analysis of the least square method. The best-fit curve with the optimized values of n, m_1, m_2 is also denoted in Fig. 2(a). The two characteristic features can be derived from these analyses: the power law type swelling equation can be applied in a wide range of volumetric swelling from 0.58% (87 dpa) to 6.3% (107 dpa), and thus extrapolation is made from 107 to 120 dpa using linear log–log plot representation within the swelling transient region.

In order to study the possibility of application of the power law swelling correlation, swelling data of the 20% cold-worked 316 were analyzed with the same method. The following data base are included in this study based

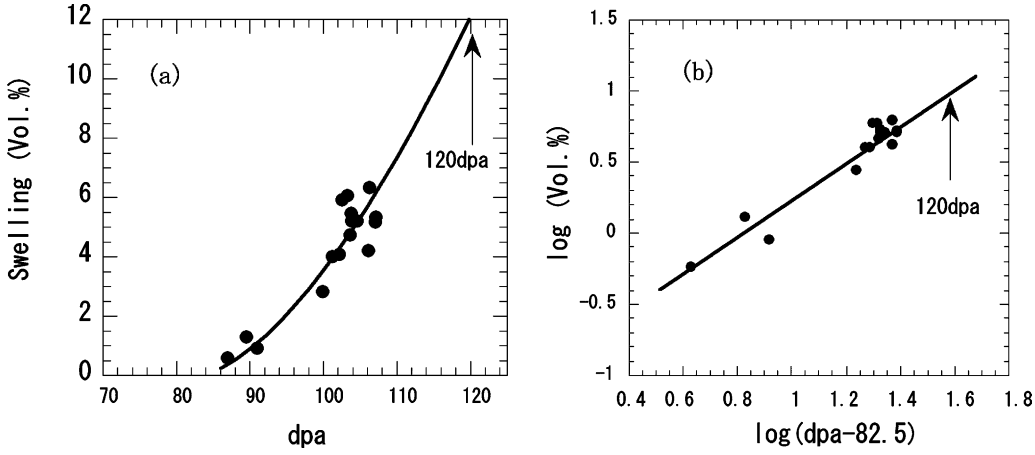

Fig. 2. Swelling expression of PNC316 in linear and log–log relation for neutron dose in the temperature range of 465–505 °C.

on the already published literatures: French 20% cold-worked 316Ti [6], 20% cold-worked AISI 316 stainless steels R-lot [2], 4th core lot [7] and N-lot [7] irradiated in FFTF and model alloys of Fe–15Cr–12Ni and Fe–16Cr–16Ni [7] as a reference. All of these swelling data including PNC316 are plotted in Fig. 3 as a function of neutron dose. Fig. 4 summarizes all of these data in log–log plot for volumetric swelling versus neutron dose. It is shown that there is linear relationship in the wide range of swelling for each alloy. In this analysis, the values of n, m_1, m_2 were optimized for each alloy using a regression analysis of the least square method. In the case of FFTF 4th core, N-lot and model alloys, n-values become near one corresponding to the steady state swelling

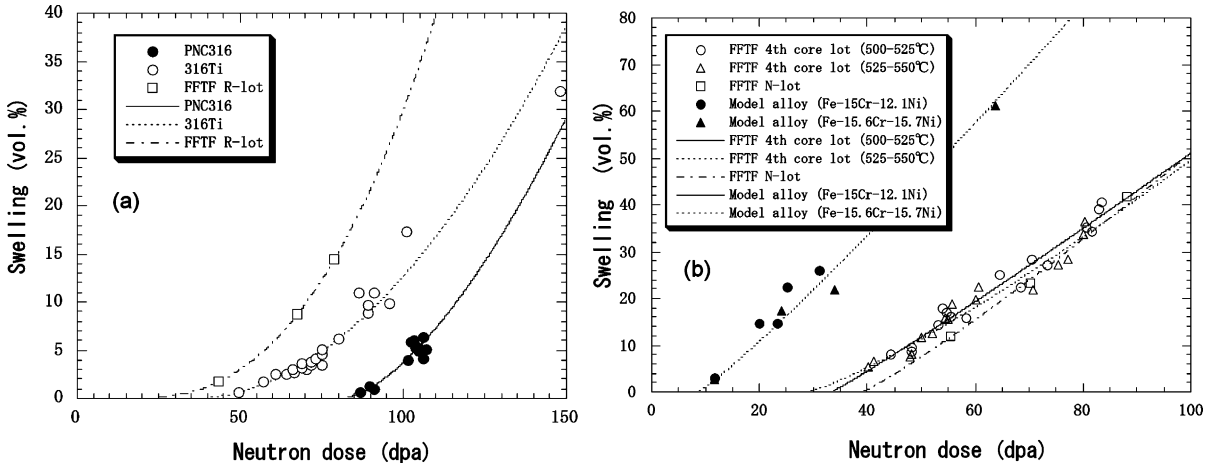

Fig. 3. Swelling versus neutron dose for typical 20% cold-worked 316 and model alloys. Note that in right hand side figure vertical axis is enlarged double and horizontal axis is reduced two-third.

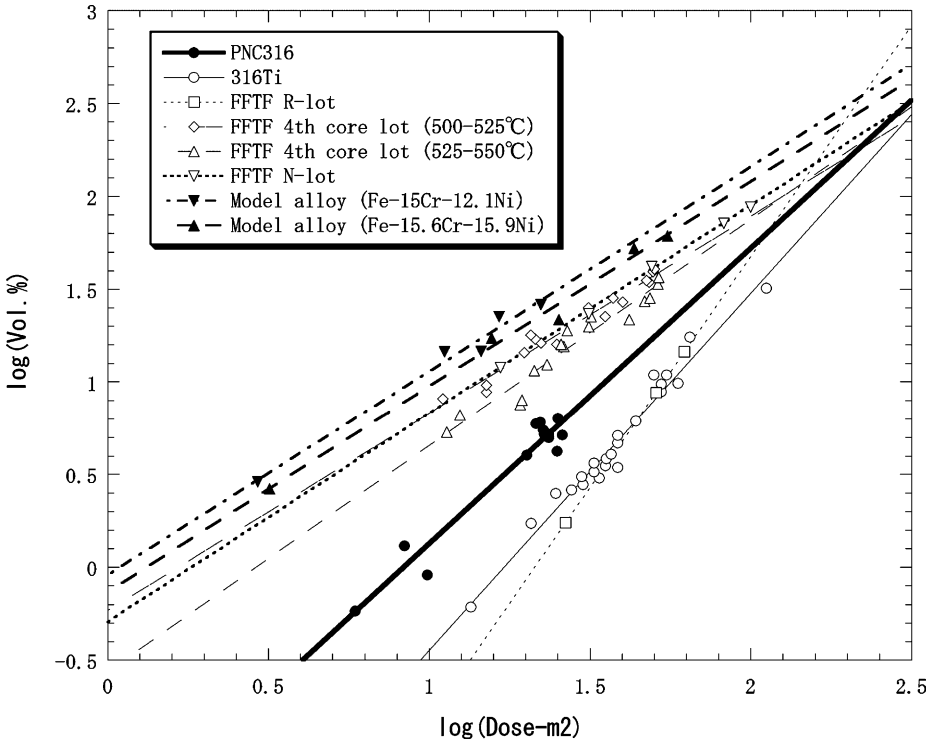

Fig. 4. Log–log plot for swelling versus neutron dose for typical 20% cold-worked 316 and mode alloys.

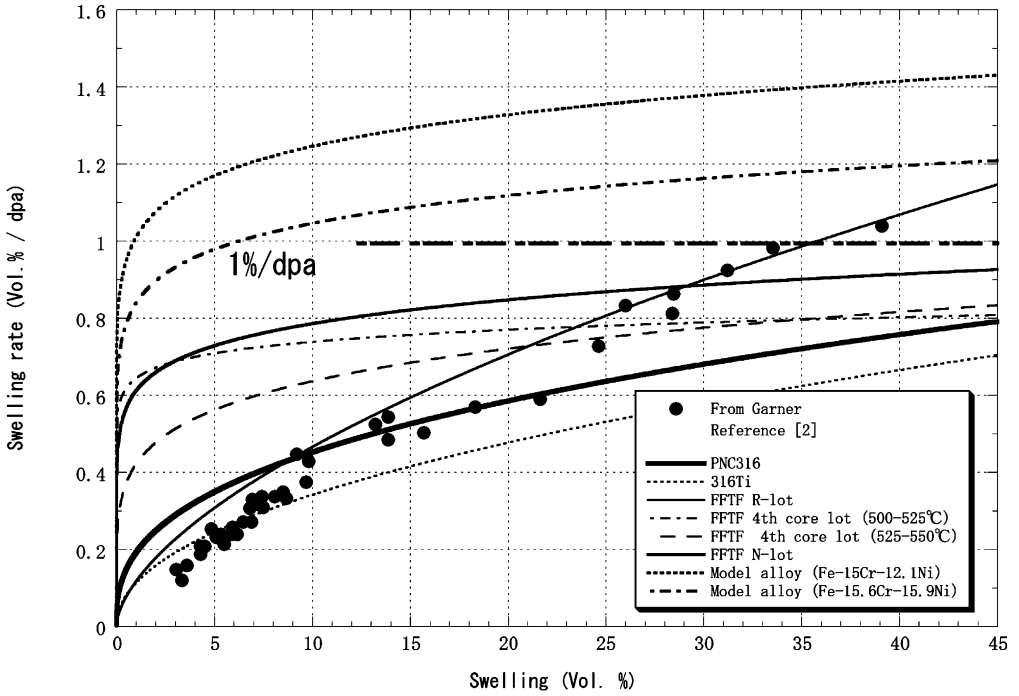

Fig. 5. Swelling versus swelling rate relation for typical 20% cold-worked 316 and model alloys, predicted by means of power law swelling equation. Garner's data are also over-plotted.

region, while PNC316, 316Ti and FFTF R-lot exhibit n-values larger than one that shows still transient swelling region in these materials. The transformed curves from log–log plot into linear volumetric swelling versus neutron dose are also denoted in Fig. 3.

On the basis of power law swelling equation (1), volumetric swelling rate is derived as Eq. (2):

$$\mathrm{d}(\Delta V/Vo)/\mathrm{d}(\phi t) = n m_1^{1/n} (\Delta V/Vo)^{(1-1/n)}. \tag{2}$$

Using Eq. (2), correlation of volumetric swelling versus swelling rate was estimated and plotted in Fig. 5. In this figure, the estimated data by Garner are also shown by solid circles that were derived from the EBR-II swelling data of annealed Ti-modified 316 stainless steels at both 540 and 425 °C up to 75 dpa [2]. The correlation for FFTF R-lot just coincides with Garner's data. In the case of FFTF 4th core and N-lot, volumetric swelling rate approaches 1%/dpa at relatively low stage of the volumetric swelling of 10%. Model alloys demonstrates the rapid increase of volumetric swelling rate of 1%/dpa for the volumetric swelling of less than 5%. On the contrary, slow increase of volumetric swelling rate with increasing neutron dose appears in PNC316 and 316Ti. It is demonstrated that transient region extends at the level of higher volumetric swelling for PNC316 and 316Ti. At post-transient swelling region with higher volumetric swelling of more than 20%, the estimated swelling rate seems to be lower than expected of 1%/dpa.

3. Rate theory analysis

3.1. Rate equation considering void and dislocation sinks

In this section, we calculate the swelling in austenitic stainless steels in terms of the well known rate theory. The swelling is calculated by summation of j-class of void as

$$\Delta V/Vo = 4/3\pi \sum_j r_{cj}^3 \rho_{cj}, \tag{3}$$

where r_{cj} is void radius and ρ_{cj} is void number density for j-class. The growth rate of void determined by the net flux of vacancy per unit void area per unit time is expressed in Eq. (4), using the vacancy concentration C_v^e in thermal equilibrium with a void of radius r_c [8]

$$\frac{\mathrm{d}r_c}{\mathrm{d}t} = \frac{\Omega}{r_c}(D_v(C_v - C_v^e) - D_i C_i), \tag{4}$$

$$C_v^e = C_v^o \exp\{\Omega/kT(2\sigma/r_c - P_g)\}, \tag{5}$$

where D_v and D_i are diffusion coefficient for vacancies and interstitials, respectively, C_v, C_i and C_v^o are concentrations of vacancy, interstitial and thermal vacancy, respectively. Ω and σ are atomic volume and surface energy of void, respectively. P_g is the gas pressure in a void that was assumed to be equal to $2\sigma/r_c$, because we

consider only void growth after completion of bubble to void conversion.

The vacancy and interstitial concentrations are determined by the following rate equations at steady state [8]:

$$dC_v/dt = G_v - RC_iC_v - S_vD_vC_v, \quad (6)$$

$$dC_i/dt = G_i - RC_iC_v - S_iD_iC_i, \quad (7)$$

where G_v and G_i are production rate and R is recombination coefficient for vacancy and interstitial, respectively, which are expressed as

$$G_i = \eta G_{dpa}\Omega^{-1}, \quad (8)$$

$$G_v = \eta(1-\varepsilon)G_{dpa}\Omega^{-1}, \quad (9)$$

$$R = 4\pi(4\times10^{-10})(D_i + D_v), \quad (10)$$

where η, ε and G_{dpa} are damage efficiency, fraction of vacancy loss due to cascade collapse and damage rate, respectively. S_v and S_i are sink strength for vacancies and interstitials, respectively, and are determined using the dislocation bias for interstitials, Z_i^d [8]:

$$S_v = \rho_d + 4\pi r_c\rho_c, \quad (11)$$

$$S_i = Z_i^d\rho_d + 4\pi r_c\rho_c, \quad (12)$$

where ρ_d is the dislocation density and ρ_c is the cavity density. The basic parameters that are necessary for the calculation of void swelling are summarized in Table 1 [9]. The calculation in this study was conducted based on results of transmission electron microscopy observation for the PNC316 segment: $\rho_d = 1.37\times10^{14}$ m^{-2} and $\rho_c = 1.42\times10^{20}$ m^{-3} at 105 dpa and 525 °C in FFTF irradiation. Results of post-irradiation examination are summarized in Table 2. The dislocation density, ρ_d, was assumed to be kept at almost constant during further irradiation. A theoretical analysis of nucleation stage of bubble leads to large uncertainty. Thus, in this calculation the change of void number density, ρ_c, was fed from the results of observation by transmission electron microscopy, which corresponds to void number density after completion of bubble–void conversion. The calculation was conducted for three types of change in void number density during irradiation based on the microstructure observation as shown in Fig. 6(a) linearly increase from 80 dpa through $\rho_c = 1.42\times10^{20}$ m^{-3} at 105 dpa, (b) saturate at $\rho_c = 1.42\times10^{20}$ m^{-3} at 105 dpa and (c) spontaneous formation of void of $\rho_c = 1.42\times10^{20}$ m^{-3} at 80 dpa.

Table 1
Basic parameter used for the present calculation

Parameters	Notations	Values
Migration energy of interstitials	E_m^i	0.5 eV
Migration energy of vacancies	E_m^v	1.4 eV
Formation energy of vacancies	E_f^v	1.6 eV
Surface energy of a void	σ	7.8×10^{18} eV/m^2
Gas pressure in a void	P_g	0
Atomic volume	Ω	10^{-29} m^3
Damage efficiency	η	0.33
Fraction of vacancy loss due to cascade	ε	0
Dislocation bias for interstitials	Z_i^d	1.132

Table 2
Results of transmission electron microscopy observation at 525 °C

Items	Notations	PIE results
Dislocation density (m^{-2})	ρ_d	1.37×10^{14} (105 dpa)
Void number density (m^{-3})	ρ_c	1.42×10^{20} (105 dpa)
Phosphide number density (m^{-3})	ρ_{Fe_2P}	2.0×10^{21} (80 dpa)
		3.0×10^{20} (105 dpa)
Phosphide length (m)	L	5.0×10^{-8}
M_6C number density (m^{-3})	ρ_{M_6C}	7.4×10^{19} (80 dpa)
		1.6×10^{20} (105 dpa)
M_6C radius (m)	r_{M_6C}	3.0×10^{-8}

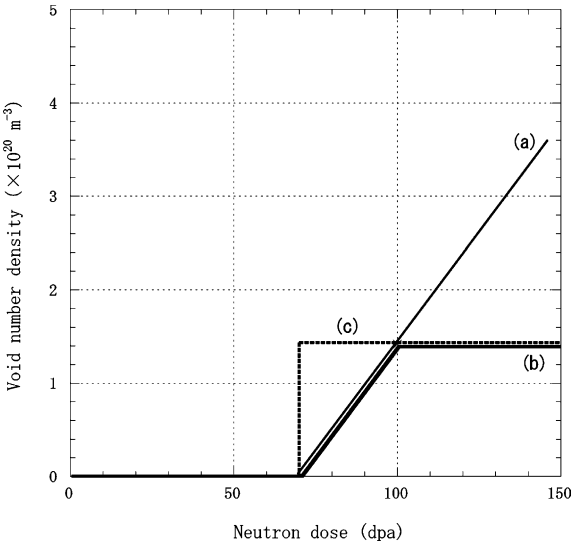

Fig. 6. Void number density change versus neutron dose that was adopted, as parameters in this calculation.

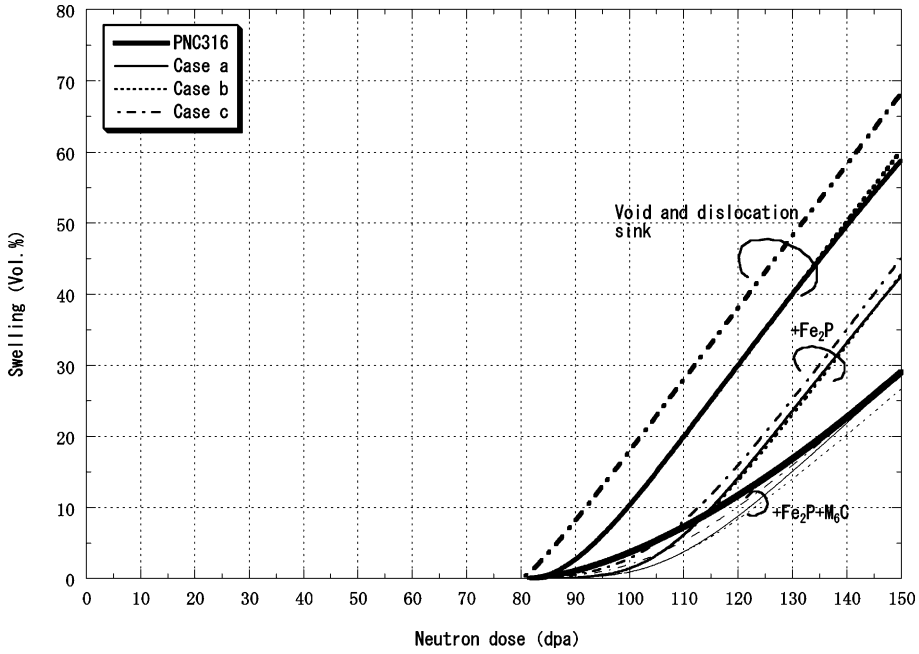

Fig. 7. Swelling versus neutron dose for PNC316, predicted by means of rate theory analysis with a parameter of three different types of sink, for evolution of void number density, case (a), (b) and (c). Swelling trend derived by power law swelling equation is also drawn.

The swelling was calculated at interval of 0.1 dpa step up to certain dpa, by putting the dislocation density of 1.37×10^{14} m^{-2}, void number density and basic parameters in Table 1 into Eqs. (3)–(12) and repeating until convergence in void radius. One proceeded such calculation forward on the next step of dpa to drive swelling trend versus neutron dose. In this calculation, Z_i^d value = 1.132 was selected for dislocation bias of interstitials so as to satisfy that swelling rate will take 1%/dpa at the final stage of steady state swelling. Results of calculation are shown in Fig. 7 by denoting void and dislocation sink. These curves contain swelling behavior corresponding to the three types of evolution of void number density. The linear increase of void number density shown in type (a) results in a slightly lower swelling than that of type (b), although void number density attains more than double at 150 dpa as shown in Fig. 6. Those results are ascribed to the suppressed void growth due to increased void number density in the type (a). The notated curves by void and dislocation sink in Fig. 8 exhibit the swelling rate–swelling correlation. It turned out that swelling rate quickly approaches 1%/dpa at the swelling level of 10%, which appears to be similar to those of FFTF 4th core and N-lot as shown in Fig. 5. On the contrary, PNC-316 clearly takes the prolonged swelling transient region. The foregoing results suggest that another sink effectively plays an important role for decreasing concentrations of vacancy and interstitials in PNC316 and 316Ti.

3.2. Effect of precipitates on swelling

Formation of needle-like phosphide is prominent in P–Ti modified PNC316. TEM observation showed that phosphide number density increases during irradiation, and attains 2×10^{21} m^{-3} at 80 dpa when swelling is just initiated. The phosphide tends to disappear in further irradiation, and fall to 3×10^{20} m^{-3} in number density at 105 dpa. The results of the observations are listed in Table 2. Based on the observation, effects of phosphide on sink strength in PNC316 can be estimated. The phosphide can be approximated as elongated ellipsoids, and sink strength of such shape is derived as [10]

$$S_{v,i} = 4\pi\rho_{Fe_2P}L/\ln(2L/N), \tag{13}$$

where ρ_{Fe_2P} is a number density of phosphide. L and N are length of the longest and shortest axes in the elongated ellipsoids, respectively. In this calculation, 50 nm were used for L value from the measurement by TEM, but N value was postulated to be 5 nm. Results of sink strength calculation are summarized in Table 3. In Fig. 9(a), the phosphide sink strength is approximated by broken curve through the measured points at 80 and 105 dpa. The denoted curves by (+Fe_2P) in Figs. 7 and 8 show the swelling versus dpa and swelling rate versus swelling relations, respectively, taking into account not only voids and dislocations but also phosphides as a radiation defect sink. The swelling rate seems to approach 1%/dpa at 20%

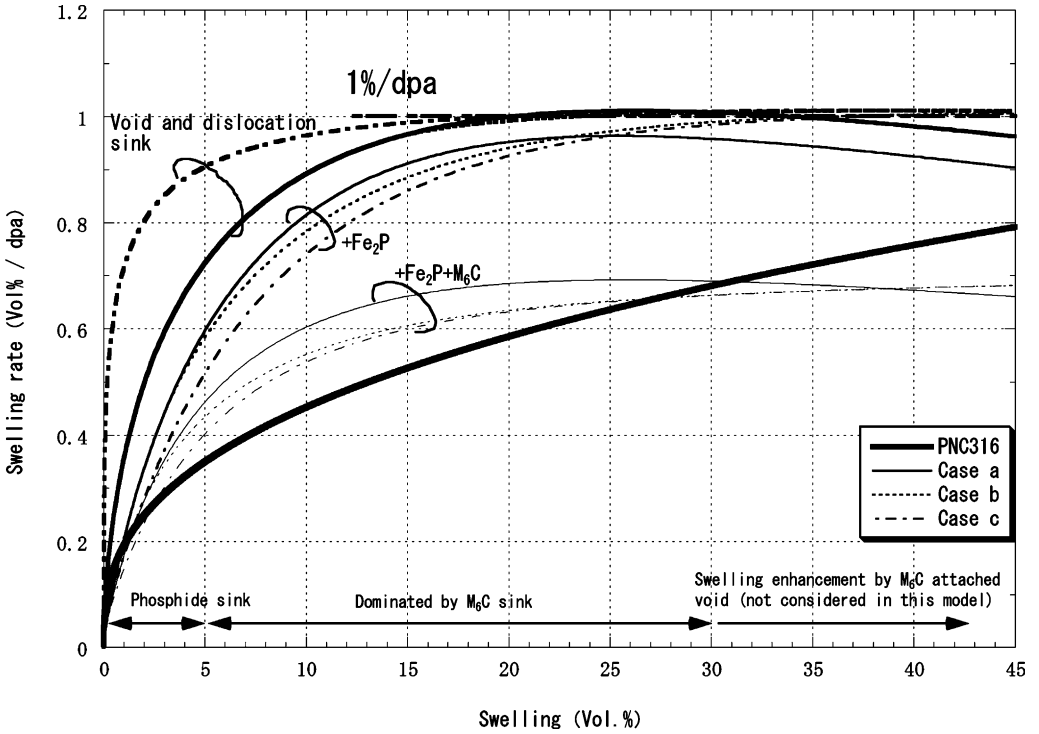

Fig. 8. Swelling versus swelling rate relation for PNC316, predicted by means of rate theory analysis with a parameter of three different types of sink, for evolution of void number density, case (a), (b) and (c). Derived by power law swelling equation for PNC316 is also drawn. Beyond 30% swelling, these calculations predict less swelling, since the model adopted did not take into account an effect of point defect collection and swelling enhancement at M_6C attached void.

Table 3
Results of sink strength calculation at 525 °C

Dislocation sink strength (m^{-2})	1.4×10^{14} (105 dpa)
Phosphide sink strength (m^{-2})	4.2×10^{14} (80 dpa)
	6.3×10^{13} (105 dpa)
M_6C sink strength (m^{-2})	3.8×10^{13} (80 dpa)
	6.8×10^{13} (105 dpa)

swelling, which is similar to results of calculation considering only dislocations and voids as a sink, since the phosphides disappear at early stage of irradiation. This result of calculation on swelling rate seems to be somewhat higher than expected of PNC316 as shown by solid curve in Fig. 8. As to dislocation sink adopted in this calculation, we supposed that dislocation density maintained the same value of 105 dpa in further irradiation. Because dislocation tends to annihilate in further irradiation, dislocation sink strength might rather decrease. Existence of a sink other than phosphide and dislocation is suggested at high swelling exceeding 10%.

We should pay attention to the carbide precipitates such as M_6C in PNC316. There are much abundance of M_6C under existing voids, of which number density and average diameter were measured by TEM. The sink strength of M_6C was expressed in Eq. (14) as an approximation of the sphere [10].

$$S_{v,i} = 4\pi r_{M_6C}\ \rho_{M_6C}, \tag{14}$$

where ρ_{M_6C} and r_{M_6C} are number density and radius of M_6C carbide. Using measured values by TEM, which are shown in Table 2, the estimated sink strength curve of summation of M_6C and phosphide is shown in Table 3 and Fig. 9(b), where sink strength of M_6C was supposed to be constant beyond 105 dpa. The denoted curves by ($+Fe_2P + M_6C$) in Figs. 7 and 8 show swelling–dpa and swelling rate–swelling relation. The calculation using the sink strength of both phosphide and M_6C carbide leads to the reasonable swelling trend up to 150 dpa and reasonable suppressed swelling rate at swelling beyond 20%, from comparison with the predicted PNC316 curve.

It is well known that an interface between phosphide and matrix is partially-coherent, and it acts as recombination site for interstitials and vacancies [11]. Formation of phosphide, thus, reduces the matrix concentration of defects and anti-defects, and causes the prolongation of swelling transient regime. However, under the

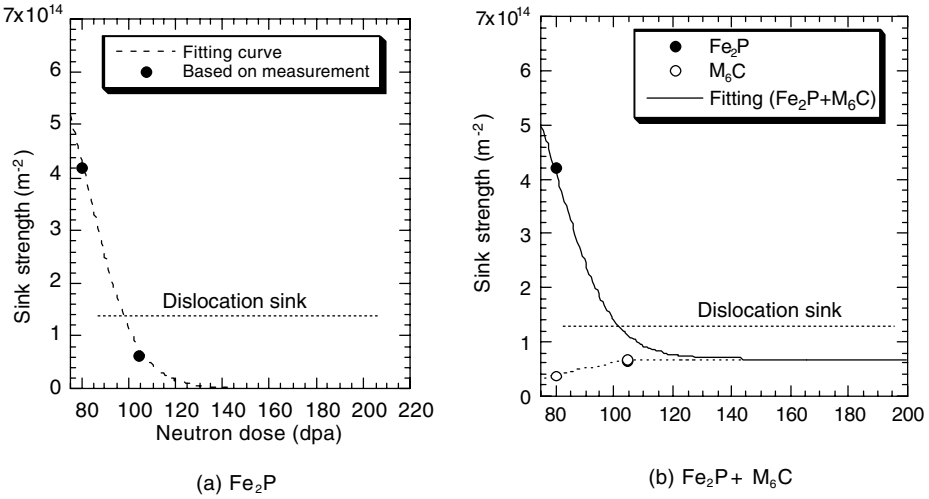

Fig. 9. Sink strength calculated based on the TEM observation of number density and size of precipitates at 80 and 105 dpa.

irradiation of PNC316, phosphide easily disappeared at the onset of swelling [12,13], which turned out to cause less effective for suppression of swelling rate and for prolongation of transient regime.

On the contrary, M_6C is incoherent precipitates and is formed by radiation-induced solute segregation (RIS) of undersize elements such as nickel and silicon. This phenomenon belongs to inverse Kirkendall effect and it is pointed out that M_6C and also G-phase are grown by replacement of MC [14,15]. Concurrently radiation induced vacancies and interstitial defects diffuse to the sink of precipitate–matrix interface [15]. Therefore, M_6C particles could serve as sink of defects and thus prolong the swelling transient regime as similar manner to phosphide. The present rate theory analyses suggested that M_6C could be rather dominant sink of radiation point defect after dissolution of phosphide. However, coarsening of M_6C precipitates causes collection of the point defects at the precipitates–matrix interface, and lead to the channel to the attached voids [16]. In the present analyses, such swelling enhancement by effect of defect collection at the interface between M_6C precipitate and matrix is not considered. The slightly enhanced swelling rate approaching 1%/dpa beyond 30% swelling in PNC316 curve, which can not be predicted in this analyses, could be attributed to the point defect collection and accelerated growth of the attached void at the void-M_6C precipitate interfaces.

4. Conclusion

From analyses of swelling in 20% cold-worked 316 stainless steels using power law type of equation, swelling rate versus swelling correlation was derived in the wide range of swelling up to 60%. In P and Ti-modified PNC316 and Ti stabilized French 20% cold-worked 316Ti, transient region of swelling is significantly prolonged and relatively low swelling rate of less than 0.6%/dpa extends up to swelling level of 20%, as compared with 20% cold-worked AISI 316 and ternary Fe–Cr–Ni model alloys. The rate theory approach considering only dislocations and voids as a sink suggested that steady state linear swelling rate approaching 1%/dpa early reached within 20% swelling regime, which coincides with the swelling behavior of 20% cold-worked AISI 316 and model alloys. For PNC316 and 20% cold-worked 316Ti, precipitates play an important role as additional sink to suppress swelling rate. Phosphides are strong sink for vacancies and interstitials, but are dissolved just at onset of swelling. The extension of low swelling rate transient region up to 20% swelling was interpreted as being due to incoherent precipitate carbides that could also absorb point defects at the precipitate–matrix interfaces through inverse Kirkendall effect.

Acknowledgements

We wish to thank Mr N. Akasaka and other members of Materials Monitoring section at O-arai Engineering Center for carrying out density measurement and TEM observation of the irradiated PNC316. The authors are also pleased to thank Mr M. Ito of Nuclear Engineering System Inc. for his assistance of this analyses.

References

[1] F.A. Garner, in: R.W. Cahn, P. Haasen, E.J. Kramer (Eds.), Materials Science and Technology, vol. 10A, 1994, p. 419.

[2] F.A. Garner, in: Proceedings of the Symposium on Optimizing Materials for Nuclear Applications, Los Angeles, Warrendale, The Metallurgical Society of AIME, 1985, p. 111.
[3] I. Shibahara, S. Ukai, S. Onose, S. Shikakura, J. Nucl. Mater. 204 (1993) 131.
[4] S. Ukai, T. Yoshitake, N. Akasaka, T. Donomae, K. Katsuyama, T. Mitsugi, T. Asaga, ANS Transaction (November) (1998) 115.
[5] J.P. Foster, D.L. Poter, D.L. Harrod, T.R. Mager, M.G. Burke, J. Nucl. Mater. 224 (1995) 207.
[6] J.-L. Seran, H. Touron, A. Maillard, P. Dubuisson, J.P. Hugot, E.Le. Boulbin, P. Blanchard, M. Pelletier, in: Proceedings of the 14th International Symposium on Effects of Radiation on Materials, ASTM-STP 1046, 1990, p. 739.
[7] F.A. Garner, M.B. Toloczko, B.H. Sencer, J. Nucl. Mater. 276 (2000) 123.
[8] L.K. Mansur, Nucl. Technol. 40 (1978) 5.
[9] R.E. Stoller, G.R. Odette, J. Nucl. Mater. 103&104 (1981) 1361.
[10] A.D. Brailsford, L.K. Mansur, J. Nucl. Mater. 103&104 (1981) 1403.
[11] H. Watanabe, T. Muroga, N. Yoshida, in: Proceedings of the 16th International Symposium on Effects of Radiation on Materials, ASTM-STP 1175, 1993, p. 951.
[12] S. Ukai, N. Akasaka, K. Hattori, S. Onose, in: Proceedings of the 18th International Symposium on Effects of Radiation on Materials, ASTM-STP 1325, 1998, p. 808.
[13] E.H. Lee, L.K. Mansur, A.F. Rowcliffe, J. Nucl. Mater. 122&123 (1984) 299.
[14] P.J. Maziasz, J. Nucl. Mater. 122&123 (1984) 472.
[15] O.V. Borodin, V.V. Bryk, V.N. Voyevodin, I.M. Neklyudov, V.K. Shamardin, V. Neystroev, in: Proceedings of the 17th International Symposium on Effects of Radiation on Materials, ASTM-STP 1270, 1996, p. 817.
[16] A.F. Rowcliffe, E.H. Lee, J. Nucl. Mater. 108&109 (1982) 306.